

Advanced Anticorrosion Coatings Prepared from Polybenzoxazine/ α -zirconium Phosphate Nanocomposites

Shuliang Li, Chunxia Zhao*, Haolan Gou, Yuntao Li*, Xiaojia He, Ling Zhao

College of Materials Science and Engineering, Southwest Petroleum University, Chengdu 610050, China

*E-mail: polychem2011@hotmail.com (C. Zhao), yuntaoli@swpu.edu.cn (Y. Li)

Received: 16 November 2017 / Accepted: 21 January 2018 / Published: 5 February 2018

In this study, we present the first successful application of polybenzoxazine/ α -zirconium phosphate (PBa/ α -ZrP) nanocomposites for corrosion protection. α -ZrP nanoplatelets were exfoliated by a polyetheramine surfactant (Jeffamine M1000), and the α -ZrP dispersed well in the PBa matrix with no substantial agglomeration. PBa/ α -ZrP composite coatings were also prepared on the carbon steel substrate, and their anticorrosive properties were investigated in 3.5 wt% NaCl solution via electrochemical impedance spectroscopy and polarization curves. The results reveal that well-dispersed α -ZrP nanoplatelets in the PBa matrix effectively enhanced the corrosion protection ability of the coatings, attributing to the extended diffusion path of the corrosive agents in the coating to reach to the protected metal surface. The samples with 5 wt% α -ZrP nanoplatelets showed a corrosion rate of 0.108 mm per year for carbon steel after 8-day immersion, and the corrosion rate was less than half of that of the neat pristine PBa sample. These results of this study reveal that the incorporation of α -ZrP in the PBa matrix efficiently improved the corrosion protection of the PBa composite.

Keywords: Polybenzoxazines; α -zirconium phosphate; Nanocomposite coatings; Anticorrosion

1. INTRODUCTION

Metallic corrosion affects the reliability of industrial facilities, causing huge economic loss and threatens the personal safety, thus prompting the study on corrosion protection for decades. Polymer matrix incorporating nanoscale filler as the reinforcements has attracted significant attention owing to their excellent barrier properties, mechanical properties, and functionalization [1–4]. The improved barrier properties of polymer/filler composites attributed to the extended diffusion path of the corrosive agents in the coating to reach the protected metal surface [5,6]. α -Zr(HPO_4)₂•H₂O (abbreviated as α -ZrP) has been considered as a promising layered nanostructure compound owing to its controllable

aspect ratio, ease of intercalation/exfoliation, and high ion-exchange capacity [7,8]. However, α -ZrP nanoplatelets have a tendency to aggregate severely as a result of the van der Waals and hydrogen bonding interactions. Since the homogenous dispersion and efficient interfacial interaction of nanofillers in organic coatings significantly affect the barrier properties of the nanocomposite coatings, α -ZrP has been widely reported to be exfoliated by various guest molecules to achieve excellent dispersion in the polymer matrix. Recently, α -ZrP-based epoxy nanocomposite [9] and polyurethane nanocomposite [10] have been prepared and confirmed to be promising anticorrosion coatings. Nevertheless, the hydroxyl groups in the epoxy backbone attribute to relatively high water uptake, and thus epoxy resins are expected to exhibit less satisfactory anticorrosion performance in aqueous environment. When heated and/or burning, polyurethane easily decomposes and releases toxic cyanate ester and atmospheric pollutants such as HCN, HCNO, N₂O, and CO₂. Therefore, the application of polyurethane is severely restricted in terms of the environmental protection and construction, necessitating the development of new resin systems.

Polybenzoxazines (PBAs), a rapidly growing class of advanced thermosetting resins, are used as superhydrophobic and anticorrosion coating materials [11–13] owing to their low water uptake, low free surface energy, zero shrinkage upon full cure, and no catalysts or a curing agent required for polymerization [14–16]. However, the micropores formed via solvent evaporation in their curing process supply diffusion channels to water, oxygen, and other corrosive ions, corroding the metal-coating interface. PBA nanocomposite coatings are expected to have relatively slower anticorrosion behavior when compared to neat polymer coatings, attributed to the increased barrier properties of the composites. In previous studies, we investigated the curing behavior, thermal stability, and flame retardancy of PBA/ α -ZrP nanocomposites [17,18]. These nanocomposites possess a relatively lower ring-opening polymerization temperature compared to the original Ba monomers and have excellent thermal stability and flame retardancy.

In this study, PBAs containing 3, 5, and 10 wt% of α -ZrP nanoplatelets were first prepared. The α -ZrP nanoplatelets dispersed in the PBA matrix were characterized by transmission electron microscopy (TEM), scanning electron microscopy (SEM), energy-dispersive X-ray (EDX) spectroscopy, and X-ray diffraction (XRD) analyses. Then, the as-prepared PBA/ α -ZrP nanocomposites were drop cast on the carbon steel surface to investigate their corrosion protection performance. The anticorrosion performance of the PBA/ α -ZrP nanocomposites was investigated by potentiodynamic polarization and electrochemical impedance spectroscopy (EIS). The rust products beneath the coatings after 8-day immersion in 3.5% NaCl solution were also investigated by XRD, SEM, and EDX spectroscopy.

2. EXPERIMENTAL

2.1. Materials

Zirconyl chloride (ZrOCl₂•8H₂O, 98%, Sigma-Aldrich), phosphoric acid (H₃PO₄, 85%, EM Science), Jeffamine M1000 polyetheramine (Huntsman Chemical), acetone (ACS grade, EM Science),

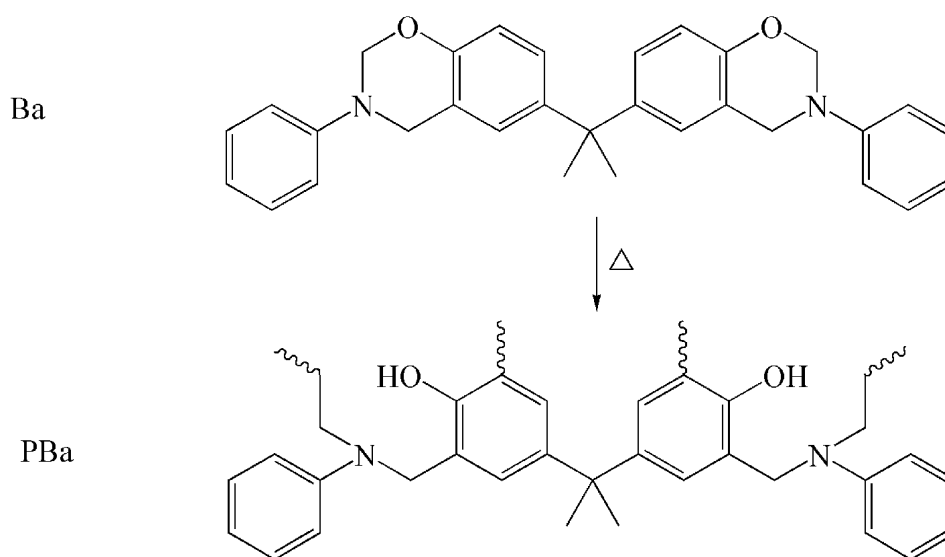
bisphenol A/aniline-based benzoxazine XU 35610 (Ba, Huntsman Chemical) were used as received without further purification.

2.2. Synthesis and exfoliation of α -ZrP

α -ZrP nanoplatelets were synthesized following our previously reported method [17,18]. 10 g of $\text{ZrOCl}_2 \cdot 8\text{H}_2\text{O}$ was refluxed in 100.0 mL of 3.0 M H_3PO_4 for 24 h. The raw product was then resuspended in de-ionized (DI) water and centrifuged three times. Subsequently, the obtained α -ZrP was dried at 65 °C for 24 h and ground to flour. Jeffamine M1000 was used to exfoliate α -ZrP in a 1:1 molar ratio of α -ZrP/Jeffamine M1000. Specifically, 1 g α -ZrP was ultrasonically dispersed in 50 mL acetone for 1 h, and later 5.6 mL of acetone containing 3.36 g Jeffamine M1000 was added dropwise to the α -ZrP dispersion. The mixture was then stirred for 12 h, ultrasonically dispersed for 1 h, and centrifuged at 10,000 rpm for 0.5 h, and finally centrifuged at 20,000 rpm for 2 h. The supernatant liquid was removed, and the gel containing exfoliated α -ZrP was collected.

2.3 Preparation of PBa/ α -ZrP nanocomposites

30 mL of acetone containing 9.7 g Ba was added dropwise to 15 mL of a 20 mg/mL exfoliated α -ZrP dispersion while stirring. The dispersion was stirred for 6 h, and then concentrated using a rotary evaporator. The obtained product was labeled as Ba/ α -ZrP-3%. Ba/ α -ZrP-5% and Ba/ α -ZrP-10% were prepared following the same method. The obtained Ba nanocomposites were cured at 180 °C for 2 h, and 200 °C for 2 h to form PBa/ α -ZrP nanocomposites, designated as PBa/ α -ZrP-3%, PBa/ α -ZrP-5%, and PBa/ α -ZrP-10%. The chemical structure and the ring-opening polymerization of Ba are shown in Scheme 1.



Scheme 1. Chemical structure of Ba and PBa.

2.4 Preparation of PBa/ α -ZrP nanocomposite coatings

The Q235 carbon steel samples ($10 \times 10 \times 1 \text{ mm}^3$) were first cleaned and degreased with acetone. The viscous dichloromethane solution containing Ba/ α -ZrP with a concentration of 0.5 mg mL^{-1} was then drop cast onto the substrate, resulting in the formation of a solid film after the evaporation of the volatile solvent at $50 \text{ }^\circ\text{C}$. The PBa/ α -ZrP coated electrode was obtained subsequently by heating the PBa/ α -ZrP-covered working electrode at $180 \text{ }^\circ\text{C}$ for 2 h and $200 \text{ }^\circ\text{C}$ for 2 h. AB Glue (Zhongshan Michel Chemical Co., Ltd, China) was used for sample sealing.

2.5 Instruments and characterizations

The nanoscopic dispersion states of α -ZrP in the PBa matrix were investigated by TEM (JEOL 2010) operated at an accelerating voltage of 200 kV. The samples were ultramicrotomed into 50–100 nm slices using a diamond knife. The morphologies of the coating surface and the rust layer on the steel substrate were observed using a Zeiss EVO MA15 scanning electron microscope coupled to an EDX spectrometer. XRD patterns of the polymer coatings and rust production were recorded by powder XRD on Philips X'pert pro MPD equipped with Cu K α radiation ($\lambda = 0.15406 \text{ nm}$). The mechanical strength was investigated using model Q-800 TA dynamic mechanical analyzer at a fixed frequency of 1 Hz and a temperature sweep of $3 \text{ }^\circ\text{C}$ per step, in the temperature range from 30 to $240 \text{ }^\circ\text{C}$. The dimensions of specimens were $40 \times 10 \times 3.2 \text{ mm}^3$. The dynamic storage modulus (G') and loss $\tan\delta$ curves against temperature were plotted. The temperature at which the $\tan\delta$ curve shows a maximum peak is recorded as T_g .

The corrosion protection performance of the PBa/ α -ZrP nanocomposite coatings was characterized by the potentiodynamic polarization and EIS using an Autolab PGSTAT302N. 3.5 wt% NaCl aqueous solution, Ag/AgCl electrode (saturated KCl), and Pt wire were used as the electrolyte, reference electrode, and counter electrode, respectively. In linear polarization experiments, the potential was scanned at a scan rate of 2 mV s^{-1} from -250 mV to $+250 \text{ mV}$ above the corrosion potential (E_{corr}), at the open circuit potential in the steady state. In impedance measurements, a 10 mV perturbation in the frequency range from 100 kHz to 0.01 Hz was applied.

3. RESULTS AND DISCUSSION

3.1. Characterization of PBa/ α -ZrP composite coatings

The XRD diffractograms of the PBa and PBa/ α -ZrP nanocomposites are shown in Fig. 1a. The XRD diffractogram of PBa shows a typical diffraction of an amorphous polymer with a broad peak at approximately 2θ of 20° [19,20]. The nanocomposites with different α -ZrP contents exhibited the similar spectrum to that of the neat PBa. As shown in Fig. 1b, there are no reflection peaks at 11.7° , corresponding to the α -ZrP interlayer of (002) [21,22], indicating complete exfoliation.

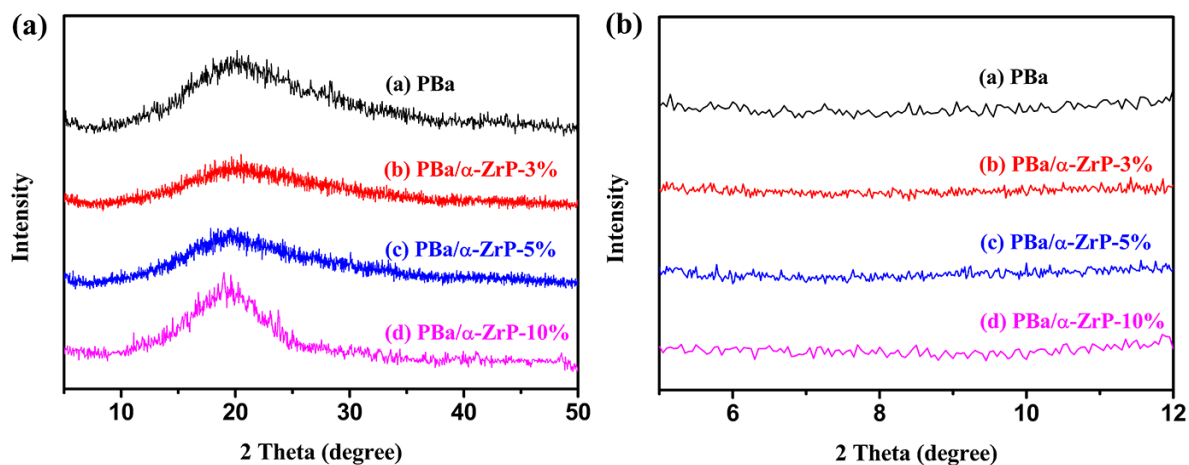


Figure 1. (a) XRD patterns of PBa and PBa/ α -ZrP nanocomposites and (b) Partial diffraction patterns of PBa and PBa/ α -ZrP.

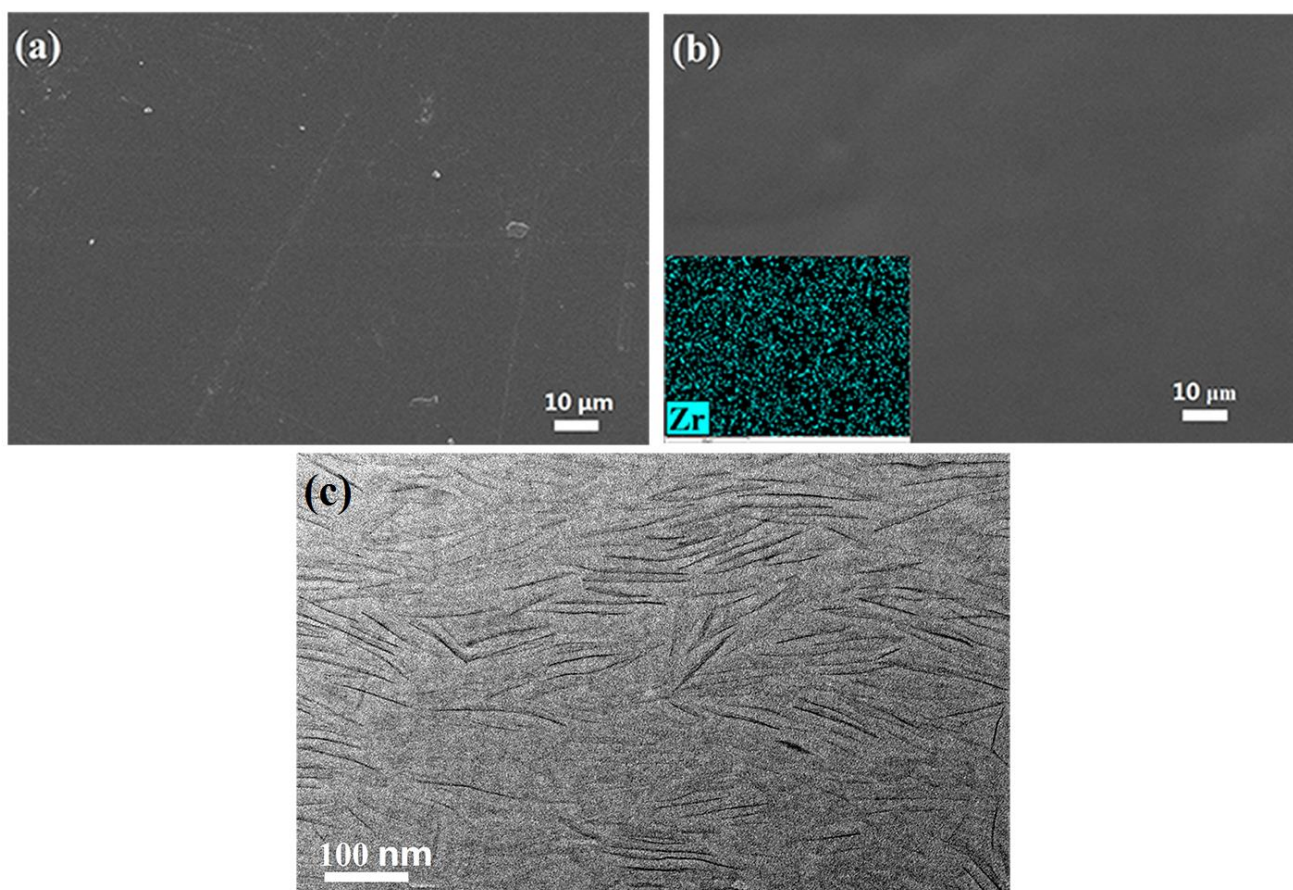


Figure 2. (a) SEM image of PBa and (b) SEM image of PBa/ α -ZrP-10%, inset of SEM image (b) shows Zr elemental mapping image from EDX spectrum for PBa/ α -ZrP-10% composite, and (c) TEM of PBa/ α -ZrP-10% nanocomposites.

The nanoscopic dispersion state of the exfoliated α -ZrP nanoplatelets in the coating matrix was determined by SEM. The surfaces of the PBa/ α -ZrP-10% composite coating (Fig. 2b) were as smooth

as that of the pristine PBa (Fig. 2a), indicating a uniform dispersion of α -ZrP nanoplatelets without agglomeration and good compatibility. The EDX mapping of zirconium (the inset in Fig. 2b) further indicated successful fabrication of PBa/ α -ZrP composites with a uniform distribution of α -ZrP. The SEM images were consistent with the TEM observations. The homogeneously dispersed α -ZrP in the composite coatings may attribute good physical barrier property to the resulting nanocomposites.

To further study the nanodispersion of α -ZrP, the morphologies of the PBa/ α -ZrP coatings were investigated by TEM. As shown in the TEM image of PBa/ α -ZrP-10% (Fig. 2c), the dark lines represent the α -ZrP nanoplatelets, and the bright area represents the PBa matrix. The exfoliated α -ZrP could be homogeneously nanodispersed in the PBa matrix without any aggregation.

3.2 Thermal dynamic mechanical characterization

The temperature-dependent dynamic mechanical plots, storage modulus and $\tan \delta$, of the neat PBa and its nanocomposites PBa/ α -ZrP are shown in Figs. 3a and 3b, respectively. The plots of storage modulus as a function of temperature in Fig. 3a show that the PBa/ α -ZrP nanocomposites slightly enhanced the dynamic storage moduli compared to that of the pristine PBa from 40 to 80 °C, attributed to the nano-reinforcement provided by the nanofiller. When the temperature exceeded 80 °C, the dynamic storage moduli of the nanocomposites were significantly lower than that of the pristine PBa and decreased with increasing concentration of α -ZrP, probably attributed to the unintended reaction [23,24] of surface modifier M1000 with the Ba monomers. Besides, the M1000 reached its melting point at 75 °C; therefore, assisted the large-scale segmental motion of the polymer. Hence, a lower temperature would be sufficient to induce the segmental motion of the PBa chains. The $\tan \delta$ plot in Fig. 3b also follows the same pattern as the storage modulus. The T_g drops from 169 °C in the case of the pristine PBa to 156, 148, and 137 °C for PBa/ α -ZrP-3%, PBa/ α -ZrP-5%, and PBa/ α -ZrP-10%, respectively, and is attributed to a large number of diethyl ether segments in M1000, in the form of flexible long chains.

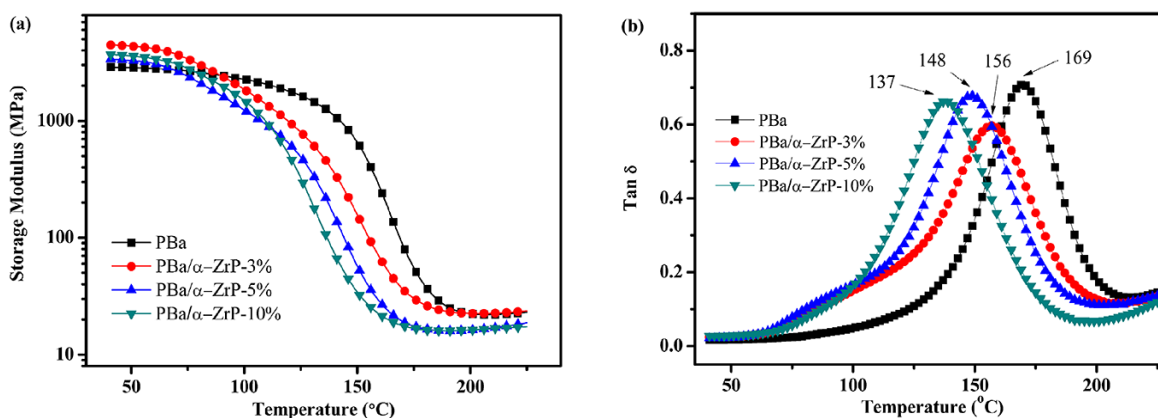


Figure 3. Temperature dependent (a) storage modulus and (b) $\tan \delta$ plots of PBa and PBa/ α -ZrP nanocomposites as obtained from DMA analysis.

3.3 Anticorrosive performance of the electrode coated with different coatings

The anticorrosion behavior of the pristine PBa and the PBa/ α -ZrP coatings was investigated by the EIS with respect to time. For the pristine PBa coating (Fig. 4a) and the PBa/ α -ZrP composite coatings (Figs. 4b–d), the radius of capacitive arcs first decreased during the initial immersion, and then increased before dropping again. The diameter of the semicircle of PBa/ α -ZrP-3% nanocomposite coatings was slightly greater than that of the pristine PBa coating after 2-day immersion, whereas those of PBa/ α -ZrP-5% and PBa/ α -ZrP-10% nanocomposite coatings were significantly larger than that of the pristine PBa coating during the whole immersion period, suggesting that the anticorrosive properties of PBa coatings improved significantly by the addition of >5 wt% α -ZrP.

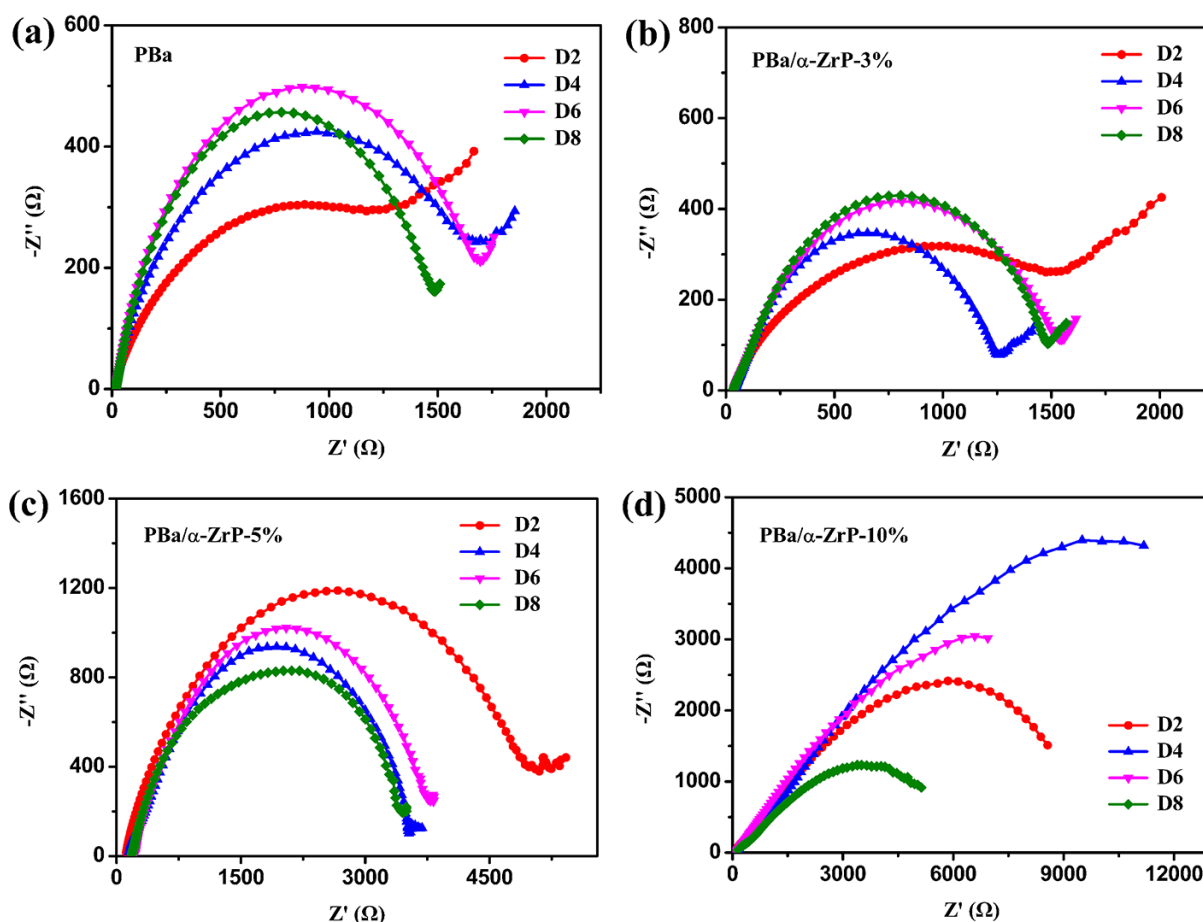


Figure 4. Nyquist plots of (a) PBa, (b) PBa/ α -ZrP-3%, (c) PBa/ α -ZrP-5%, and (d) PBa/ α -ZrP-10% coatings immersed in 3.5% NaCl solution for different times.

The impedance modulus at low frequency is another anticorrosion property evaluation index, representing the ability of the coating to impede the flow of current between anodic and cathodic areas [25–27]. Overall, the impedance modulus of the samples obviously decreased with increasing immersion time in the corrosion process. The electrolyte diffused into the coating through inherent micropores in the initial stage, but did not penetrate at the interface of steel. Subsequently, aggressive

medium (H_2O , O_2 , and Cl^-) arrived at the metal substrate and induced the corrosion reaction at the steel substrate/coating interface. As shown in the Bode impedance plot (Fig. 5), although the impedance moduli at the lowest frequency of PBa/ α -ZrP-5% and PBa/ α -ZrP-10% coatings decreased to 3.50 and 6.09 $k\Omega\text{ cm}^2$, respectively, slightly after 8-day immersion in 3.5% NaCl aqueous solution, they were still much higher than that of the pristine PBa coating. Moreover, the modulus at high frequency for the nanocomposite coatings was higher than that of the neat PBa coating by increasing immersion time to 8 days, indicating that the incorporation of exfoliated α -ZrP nanoplatelets enhanced the anticorrosion ability of the PBa coatings.

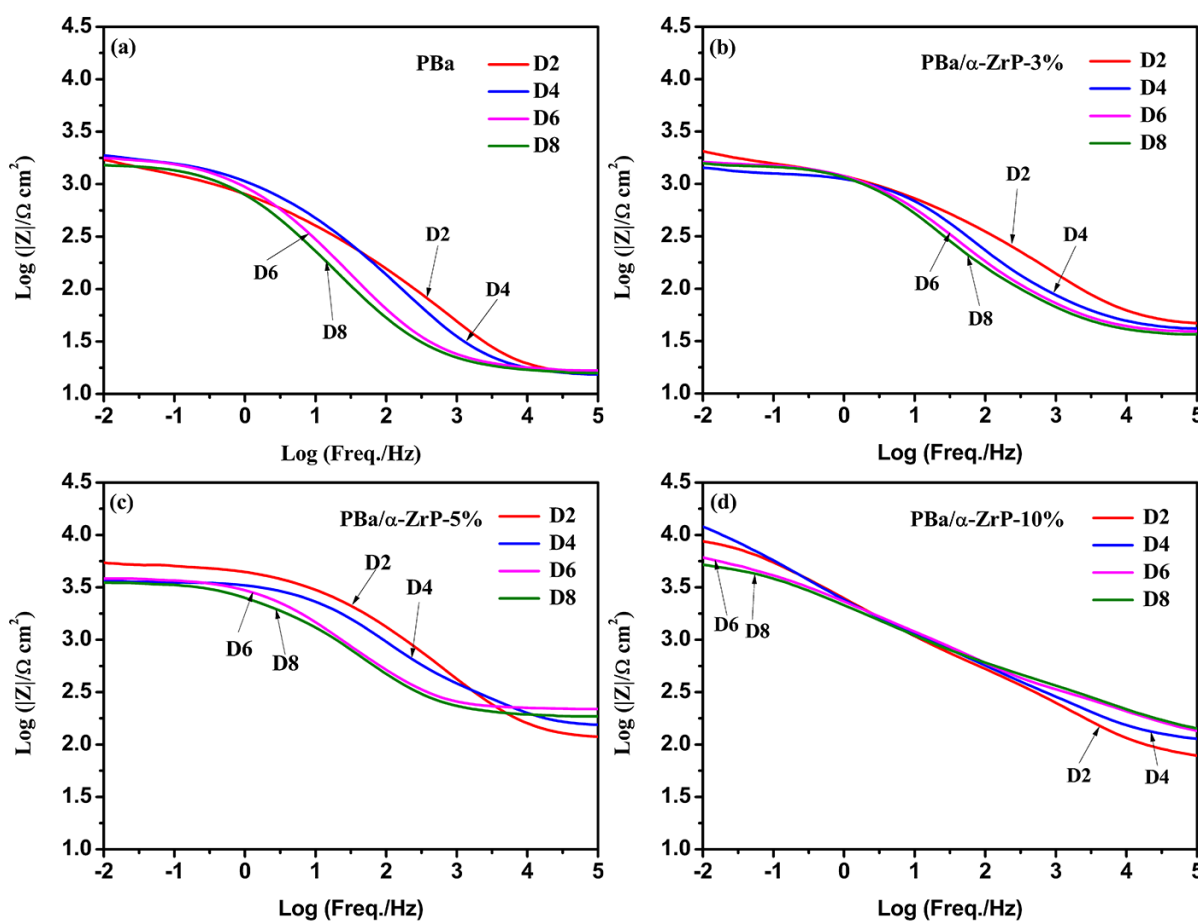


Figure 5. Time-dependent Bode modulus plots of the coating during 8-day immersion in 3.5% NaCl solution. (a) PBa, (b) PBa/ α -ZrP-3%, (c) PBa/ α -ZrP-5%, and (d) PBa/ α -ZrP-10%.

Moreover, the phase angle at high frequency is always used to evaluate the corrosion resistance ability of coatings [28–30]. As shown in the Bode phase plot (Fig. 6), the phase angle at 10^5 Hz decreased, and the peak at the high frequency shifted to a middle-high frequency region with the erosion process, indicating the gradual decline in the corrosion protection ability of the coatings. One time constant can be observed in the Bode phase plots of the pristine PBa, PBa/ α -ZrP-3%, and PBa/ α -ZrP-5% coating, indicating that the coating did not corrode during the 8-day immersion. Unlike the other coatings, PBa/ α -ZrP-10% exhibited two time constants. The time constant appearing at the high

frequency range is associated to the coating layer, whereas that at the low frequency range can be attributed to the corrosion occurring at the metal/coating interface. The dramatic decrease in time constant reveals that the barrier properties of PBA/ α -ZrP-10% coating deteriorated quickly, indicating that the corrosion occurred at the interface of the substrate metal and organic coatings. Though the exfoliated α -ZrP nanoplates dispersed in nanocomposite coatings act as a solid barrier against foreign molecules, the functional groups of the cationic surfactants (Jeffamine M1000 polyetheramine) make it hydrophilic, and increased exfoliated α -ZrP content in the composite coatings may increase the penetration of the electrolyte in the organic coatings.

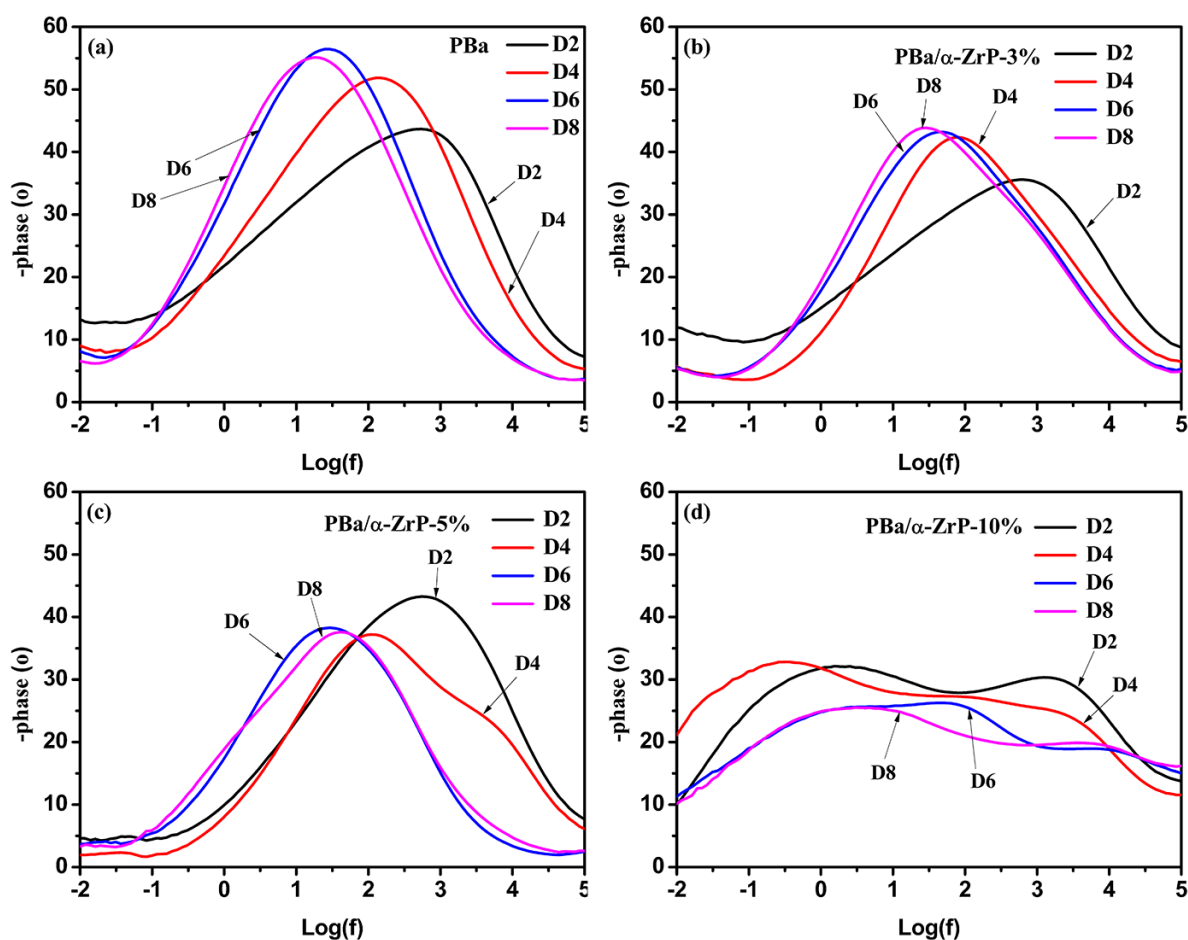


Figure 6. Time-dependent Bode phase plots of the coatings during 8-day immersion in 3.5% NaCl solution. (a) PBA, (b) PBA/ α -ZrP-3%, (c) PBA/ α -ZrP-5%, and (d) PBA/ α -ZrP-10%.

Equivalent electrical circuits are used to analyze the Nyquist plot, as they allow a more accurate fit to the experimental results. In the circuits, the R_s , R_c , Z_w , and R_{ct} represent the solution resistance, coating resistance, Warburg impedance, and charge transfer resistance of the corrosion reaction on the steel substrate, respectively [31–34]. Model a (Fig. 7a) was used to analyze the impedance data obtained from the initial stage of immersion, when the coatings efficiently acted as a barrier layer. However, this equivalent circuit could no longer provide a satisfactory fitting result with

the elapse of time. As the electrolyte solution, water and oxygen gradually penetrated through the coating and even arrived at the coating/substrate interface, a different equivalent circuit Model b taking account of the appearance of electrochemical corrosion reaction at the metal interface was used, as shown in Fig. 7b. Specifically, the C_{dl} in parallel with the R_{ct} in model b represents the Faradic reaction. In terms of the coating system where diffusion impedance appeared, Model c (Fig. 7c) was adopted to fit the impedance data. The Warburg diffusion behavior attributed to the deterioration of the coating protection and the continual diffusion in the coating system. Based on these fitting models, R_c and C_c of different coatings at a function of immersion time are shown in Fig. 8. The R_c gradually decreased with immersion time and is another evident sign for the invalidated resistance against corrosive species transfer through the pores of coating. Besides, the C_c increased with prolonging immersion time, because of the higher local dielectric constant of water than that of the polymer. PBa/ α -ZrP-5% and PBa/ α -ZrP-10% coatings exhibited higher R_c values, suggesting that the incorporation of >5 wt% α -ZrP in the PBa matrix effectively decreased the corrosion reactions on the coated metal surface. Further, the C_c value of nanocomposite coatings is relatively lower compared to the pristine PBa coatings in the whole period of immersion. Specifically, the C_c value showed an upward trend for the pristine PBa, PBa/ α -ZrP-3%, and PBa/ α -ZrP-5% coating during the extending immersion time, because of the delamination of coating. Unlike other coatings, the C_c value of PBa/ α -ZrP-10% coatings fluctuated and can be ascribed to the saturation of the hydrophilic structure of the polyetheramine and the decrease in the hydrophilic tendency of nanocomposite coatings. The fluctuation in R_c could be attributed to the accumulation of corrosion products in the coating pores [35], whereas the R_c values of PBa/ α -ZrP-5% decreased to a stable value, opposite to its C_c , by increasing immersion time. For instance, PBa/ α -ZrP-5% reached the minimum value for R_c (3.37 kohm cm^2) and maximum value for C_c ($2.40 \times 10^{-7} \text{ F cm}^{-2}$) at 8 days, exhibiting much higher R_c values and lower C_c values compared to those of the pristine PBa coating. Thus, the incorporation of 10 wt% α -ZrP endowed the PBa with better corrosion protection ability, but did not provide long term corrosion resistance. The best corrosion protection was obtained for the nanocomposite system with 5 wt% α -ZrP.

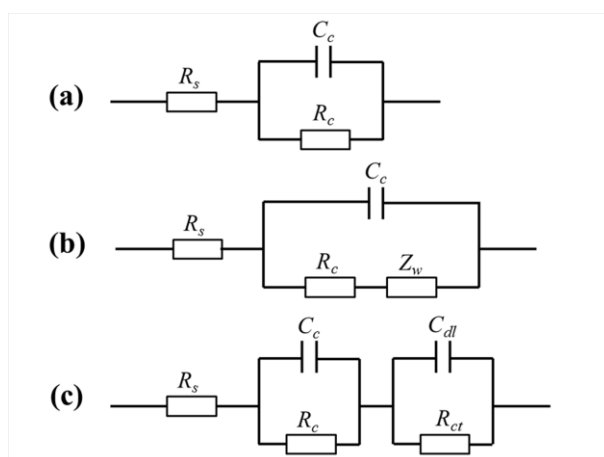


Figure 7. Equivalent electric circuits represent three different coating systems immersed for different times.

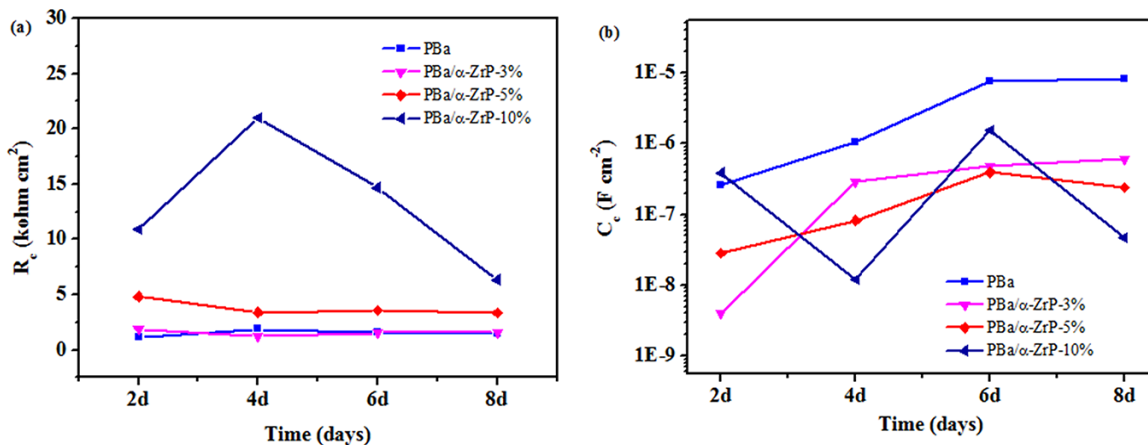


Figure 8. (a) Coating resistance, and (b) coating capacitance with immersion.

Fig. 9 exhibits the Tafel plots measured in 3.5 wt.% aqueous NaCl solution. The polarization data of the nanocomposite coated Q235 electrode with different α -ZrP mass fractions are listed in Table 1. PBa/ α -ZrP-5% covered carbon steel exhibited a more positive shift in the corrosion potential (E_{corr}) than the pristine PBa and other PBa/ α -ZrP composite coated steels. In terms of the corrosion current (I_{corr}), the lower I_{corr} always corresponds to better anticorrosive performance. The I_{corr} value of PBa/ α -ZrP-5% coated sample ($9.3073 \mu\text{A cm}^{-2}$) was lower than those for the other samples.

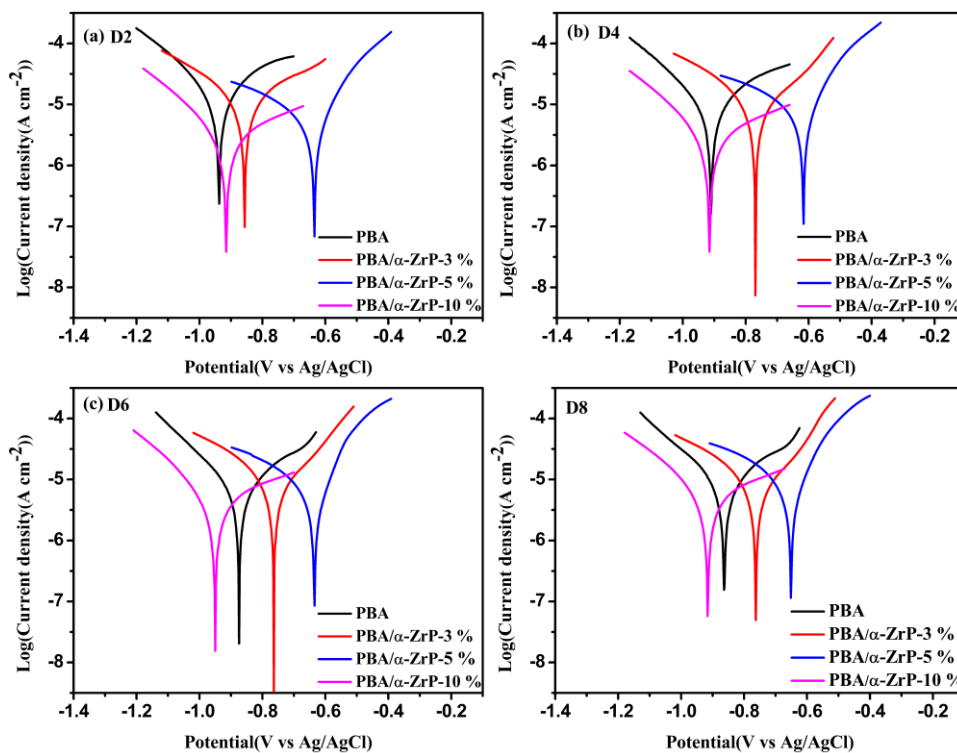


Figure 9. Tafel plots for different samples in 3.5 wt% NaCl solution for different immersion times. (a) 2 days, (b) 4 days, (c) 6 days, and (d) 8 days.

Table 1. Results of electrochemical corrosion measurements for different samples in 3.5 wt% NaCl solutions with different immersion times.

Sample	Time	E_{corr} (mV)	I_{corr} ($\mu\text{A}/\text{cm}^2$)	R_{corr} (mm/year)
PBa	2 days	-938.58	21.20	0.24
	4 days	-910.95	13.24	0.15
	6 days	-875.07	11.22	0.13
	8 days	-863.80	23.43	0.27
PBa/ α -ZrP-3%	2 days	-857.40	179.13	2.08
	4 days	-769.99	52.13	0.61
	6 days	-764.60	17.81	0.21
	8 days	-763.42	22.34	0.26
PBa/ α -ZrP-5%	2 days	-636.10	6.53	0.08
	4 days	-617.66	8.77	0.10
	6 days	-635.85	5.23	0.06
	8 days	-651.85	9.31	0.11
PBa/ α -ZrP-10%	2 days	-915.97	10.93	0.13
	4 days	-915.97	8.60	0.10
	6 days	-950.96	6.28	0.07
	8 days	-916.16	52.39	0.61

Furthermore, the decreasing corrosion rate (R_{corr}) [36,37] of PBa/ α -ZrP-10%, PBa, PBa/ α -ZrP-3%, and PBa/ α -ZrP-5% coating to 0.61, 0.27, 0.26, and 0.11 mm year⁻¹, respectively, also confirmed improved anticorrosive performance of PBa/ α -ZrP-5% coating. The PBa/ α -ZrP-10% covered electrode showed less effective corrosion protection behavior than other samples with an I_{corr} of 0.524 $\mu\text{A cm}^{-2}$ and an E_{corr} of -924.1 mV, indicating that the excessive addition of exfoliated α -ZrP addition to the PBa matrix may not efficiently hinder the diffusion pathways of oxygen and water molecules to the carbon steel surface, because of the hydrophilic groups of the polyetheramine in the exfoliated α -ZrP. Hence, PBa/ α -ZrP-5% coatings showed the best anticorrosion resistance with the balance between the micropores filling efficiency and water resistance. The following investigations were based on the samples coated with PBa/ α -ZrP-5%.

3.4 Characterization of corrosion products

The morphology of the rust products on the steel substrate coated by the pristine PBa and PBa/ α -ZrP-5% coatings after 8-day immersion is shown in Figs. 10 and 11, respectively. The pristine PBa covered steel showed the formation of cracks and needle-like corrosion product on the surface; however, the steel substrate coated with PBa/ α -ZrP-5% composite coating shows scratches on the substrate, because of the pre-polishing of the sand papers together with regular particles stacking layer-by-layer on the metal substrate. Besides, the EDX of the pristine PBa covered carbon steel (The inset Table in Fig. 10) shows O, Na, Cl, and Fe elements with the weight percentages of 11.97, 1.07, 0.22, and 81.14%, respectively. The presence of Na and Cl atoms confirmed that the corrosion reaction occurred at the steel substrate surface in 3.5% NaCl solution; however, the EDX of PBa/ α -ZrP-5%

composite covered carbon steel (The inset Table in Fig. 11) shows O, Na, Cl, and Fe elements with the weight percentages of 0.28, 0.00, 0.06, and 94.54%, respectively.

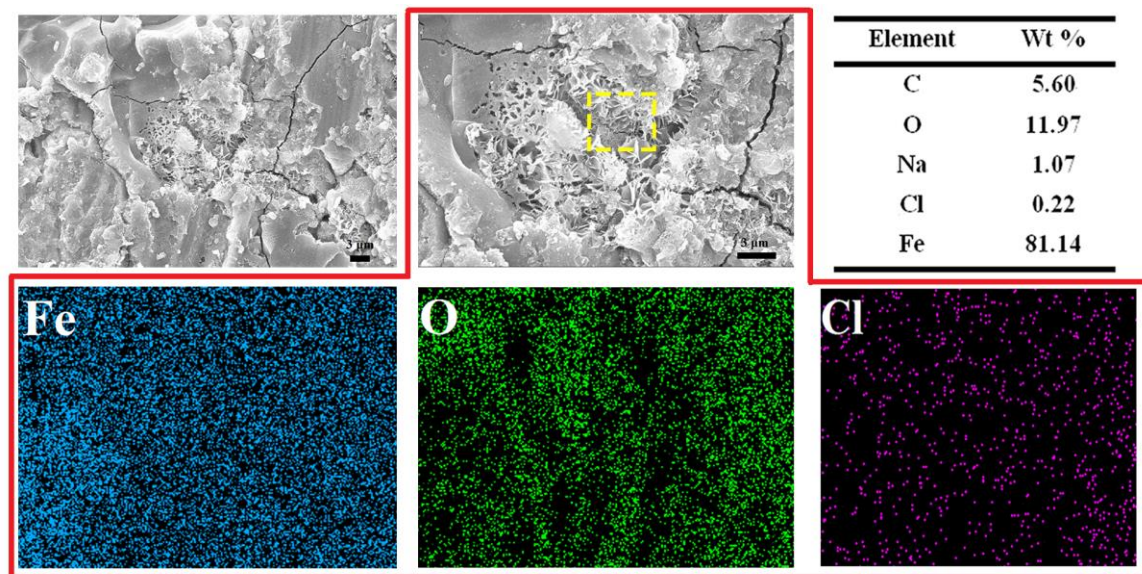


Figure 10. SEM images, elemental distribution mappings and EDX data (stem from yellow frames) of rust regions previously coated by PBA.

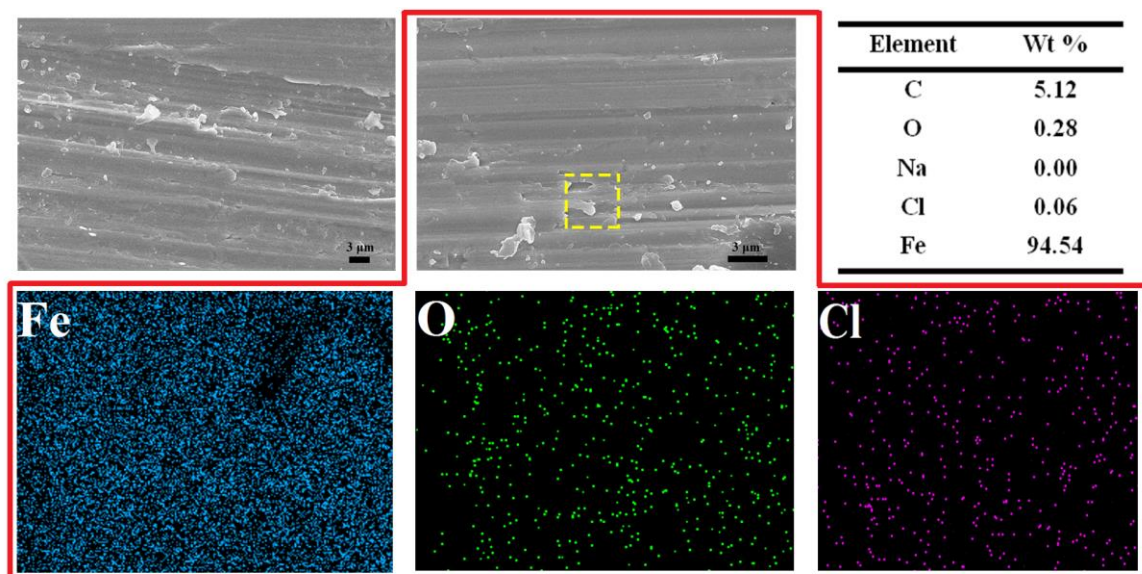


Figure 11. SEM images, element distributions mapping and EDX data (stem from yellow frames) of rust regions previously coated by PBA/α-ZrP-5%.

The metal surface covered by PBA/α-ZrP-5% coatings possessed lower concentration of O and Cl elements than that of the neat PBA, indicating that the incorporation of exfoliated α-ZrP into the PBA matrix effectively improved the corrosion protection ability of the coatings.

The components of the corrosion products on the metal substrate were further investigated by the analysis of the XRD patterns. The rust products exhibited weak diffraction peaks as a result of the strong peaks of steel substrate in the regions. As shown in Fig. 12, the rust products for the pristine PBA and PBA/ α -ZrP-5% coated substrate were mainly goethite (α -FeOOH), lepidocrocite (γ -FeOOH), and akaganeite ($\text{Fe}_2(\text{OH})_3\text{Cl}$), and $\text{Fe}_2(\text{OH})_3\text{Cl}$ was formed because of the penetration of the enriched halogen ions (Cl) through the coatings.

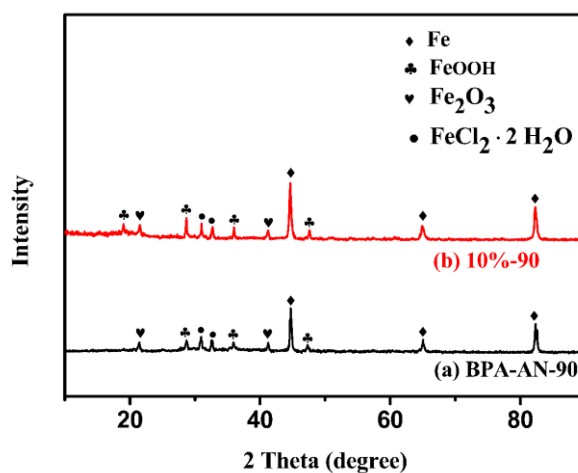


Figure 12. XRD patterns of surface of steel coated by (a) PBA, (b) PBA/ α -ZrP-5%.

4. CONCLUSION

We successfully prepared multifunctional PBA/ α -ZrP nanocomposite coatings, ideally suitable for field applications, where high corrosion resistance is required. The exfoliated α -ZrP nanoplates dispersed well in the PBA matrix, and no substantial agglomeration occurred as evidenced by the XRD, SEM, EDX, and TEM analyses, attributing to the homogeneous nanoscopic dispersion of the exfoliated α -ZrP nanoplates and the extended diffusion path of corrosive agents to reach the protected metal surface. The incorporation of α -ZrP significantly enhanced the corrosion protection performance of PBA coatings as proven by the potentiodynamic polarization curves and EIS analysis. Further, PBA/ α -ZrP-5% exhibited upper impedance modulus, more positive E_{corr} , lower I_{corr} , and declined R_{corr} during the 8-day immersion, while the pristine PBA coating did not show the same result under the same test conditions. The morphologies of the corrosion products were investigated by SEM, and the elemental components were measured by XRD and EDX. Overall, the incorporation of α -ZrP in the PBA matrix can enhance the anticorrosive properties of PBA composites.

ACKNOWLEDGEMENTS

This study was financially supported by the National Natural Science Foundation (51703191) of China, the Scientific Research Innovation Team of University in Sichuan Province (16TD0009), P. R. China, and the Foundation for Key Lab of Oil and Gas Material of Southwest Petroleum University (X151517KCL11), P. R. China.

References

1. H. Di, Z. Yu, Y. Ma, *J. Taiwan Inst. Chem. Eng.*, 64 (2016) 244.
2. Y. Ye, W. Liu, Z. Liu. *Int. J. Electrochem. Sci.*, 12 (2017) 9944.
3. Q. Niu, Z. Li, X. Yan, *Int. J. Electrochem. Sci.*, 12 (2017) 10259.
4. M. Bagherzadeh, H. Haddadi, M. Iranpour, *Prog. Org. Coat.*, 101 (2016) 149.
5. M. Nematollahi, M. Heidarian, M. Peikari, *Corros. Sci.*, 52 (2010) 1809.
6. L. A. Dobrzański, K. Lukaszewicz, A. Zarychta, *J. Mater. Process. Technol.*, 164 (2005) 816.
7. L. Chen, D. Sun, J. Li, *Mater. Des.*, 122 (2017) 247.
8. B. Pan, J. Ma, X. Zhang, *Microporous Mesoporous Mater.*, 223 (2016) 213.
9. P. Li, X. He, T. C. Huang, *J. Mater. Chem. A* 3 (2015) 2669.
10. T. C. Huang, G. H. Lai, C. E. Li, *RSC Adv.*, 7 (2017) 9908.
11. C. Zhou, X. Lu, Z. Xin, *Prog. Org. Coat.*, 76 (2013) 1178.
12. S. C. Lin, C. S. Wu, J. M. Yeh, *Polym. Chem.*, 5 (2014) 4235.
13. C. Zhou, X. Lu, Z. Xin, *Corros. Sci.*, 70 (2013) 145.
14. X. Wang, J. Wang, C. Liu, *Polym. Int.*, 67 (2017) 100.
15. K. Dogan Demir, B. Kiskan, Y. Yagci, *Macromolecules*, 44 (2011) 1801.
16. B. Wang, P. Yang, Y. Li, Y. He, *Polym. Int.*, 66 (2017) 1159.
17. C. Zhao, P. Li, D. He, *RSC Adv.*, 6 (2016) 73485.
18. J. Yue, C. Zhao, Y. Dai, *Thermochim. Acta*, 650 (2017) 18.
19. J. Wang, T. Ren, Y. Wang, *React. Funct. Polym.*, 74 (2014) 22.
20. S. Shukla, A. Ghosh, P. K. Roy, *Polymer*, 99 (2016) 349.
21. D. Yang, Y. Hu, L. Song, *Polym. Degrad. Stab.*, 93 (2008) 2014.
22. L. Sun, W. J. Boo, H. J. Sue, *New J. Chem.*, 31 (2007) 39.
23. C. S. Triantafillidis, P. C. LeBaron, T. J, *Chem. Mater.*, 14 (2002) 4088.
24. H. J. Sue, K. T. Gam, N. Bestaoui, *Chem. Mater.*, 16 (2004) 242.
25. R. Yuan, S. Wu, B. Wang, *Polymer*, 85 (2016) 37.
26. V. R. Capelossi, M. Poelman, I. Recloux, *Electrochim. Acta*, 124 (2014) 69.
27. R. Alam, M. Mobin, J. Aslam, *Appl. Surf. Sci.*, 368 (2016) 360.
28. C. Chen, S. Qiu, M. Cui, *Carbon*, 114 (2017) 356.
29. M. J. Palimi, M. Peymannia, B. Ramezanzadeh, *Prog. Org. Coat.*, 80 (2015) 164.
30. M. S. Ghaffari, R. Naderi, M. Sayehbani, *Prog. Org. Coat.*, 86 (2015) 117.
31. P. R. Kumar, D. Kalpana, N. G. Renganathan, *Electrochim. Acta*, 54 (2008) 442.
32. P. Montoya, C. R. Martins, *Electrochim. Acta*, 124 (2014) 100.
33. F. Bentiss, C. Jama, B. Mernari, *Corros. Sci.*, 51 (2009) 1628.
34. X. Liu, J. Xiong, *Prog. Org. Coat.*, 64 (2009) 497.
35. M. Golabadi, M. Aliofkhazraei, *Prog. Org. Coat.*, 105 (2017) 258.
36. J. K. Lawrence., L. O. David, *Metals Handbook of Corrosion*, ASM International, (1987), Ohio.
37. C. W. Peng, C. Hsu, K. H. Lin, *Electrochim. Acta*, 58 (2011) 614.